Journal of Materials Chemistry A

Accepted Manuscript

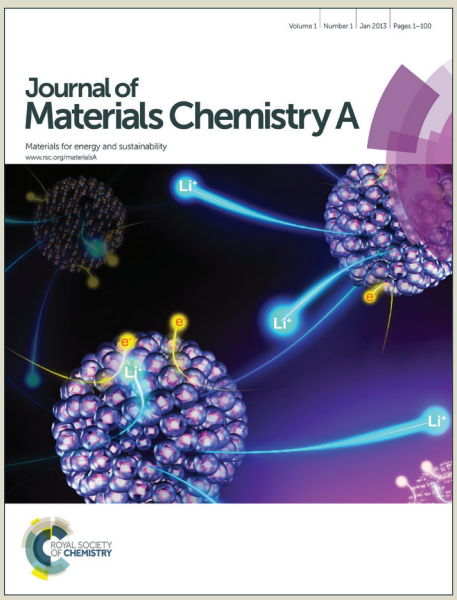

ROYAL SOCIETY OF CHEMISTRY

www.rsc.org/materialsA

Revisiting the Constructing Graphene-CdS Nanocomposites as Efficient Visible-Light-Driven Photocatalyst for Selective Organic Transformation

Zhuyun Ren, Junyu Zhang, Fang-Xing Xiao*,Guangcan Xiao*

College of Chemistry and Chemical Engineering, Instrumental Measurement and Analysis Center, Fuzhou University, Fuzhou, 350002, P. R. China.

fangxing2010@gmail.com *xgc@fzu.edu.cn*

Abstract

Cadmium sulfide (CdS) microspheres decorated graphene (GR) nanocomposite (GR-CdS) was prepared by a facile hydrothermal approach in which CdS ingredients were closely enwrapped by GR scaffold. The GR-CdS nanocomposite was subjected to a collection of characterizations including X-ray diffraction (XRD), UV-vis diffuse reflectance spectra (DRS), field emission scanning electron microscopy (FESEM), transmission scanning electron microscopy (TEM), and X-ray photoelectron spectra (XPS). It was found that integration of CdS microspheres with two-dimensional GR scaffold exert profound influence on the properties of hybrid nanocomposite, such as optical and electronic nature along with morphology. Photocatalytic performances of the GR-CdS nanocomposites were evaluated by selective organic transformation under mild conditions. The results demonstrate that the GR-CdS nanocomposite can serve as an efficient visible-light-driven photocatalyst for selective oxidation of benzyl alcohol to benzaldehyde under ambient conditions. The significantly enhanced photocatalytic performance of GR-CdS nanocomposites can be attributed to synergistic effect of enhanced light absorption intensity and high electron conductivity of GR, which facilitates charge separation and lengthens the lifetime of photogenerated electron-hole pairs. Moreover, photocatalytic performances of various GR-CdS nanocomposites featuring different degree of interfacial contact between GR and CdS were also systematically explored. It is anticipated that our work could enrich the information on the preparation of narrow bandgap semiconductor/GR hybrid nanocomposites for a wide range of photocatalytic applications.

1. Introduction

Since the pioneering work concerning photoelectrochemical water splitting on TiO_2 photoanode by Honda and Fujishima in the early 1970s, photocatalysis, as a green technique, has garnered tremendous attention and has been extensively utilized in diverse fields such as solar energy conversion, photodegradation of pollutants (*e.g.* dyes and volatile organic pollutant), water splitting, and selective oxidation.[1-12] In particular, photocatalytic selective oxidation technique demonstrates promising potential for organic synthesis on account of its facile implementation in mild conditions and the possibility to decrease the undesired environmental pollutions. Thus, enormous attention has been devoted to exploring the great potential of photocatalytic selective oxidation of various organics over copious semiconductors.[13-15]

Up to now, most of the reports on photocatalytic selective oxidation of organics over semiconductors have been focused on conventional TiO_2 or TiO_2-based nanocomposites.[13-17] However, large bandgap of TiO_2 (3.2 eV) prevents efficient absorption of sunlight in the visible region which generally results in poor overall energy conversion efficiency.[14, 18, 19] In this regard, more recently, increasing interest has been invested in developing novel visible-light-responsive photocatalysts. CdS, as a quintessential II-VI group semiconductor, has been widely studied owing to its suitable bandgap (*ca.* 2.4 eV) corresponding well to the spectrum of visible light, size-dependent electronic and optical properties,[20, 21] and demonstrated versatile applications in various fields.[22, 23 24 25, 26, 27, 28 29, 30] Nonetheless, there are still two predominant drawbacks that need to be circumvented in order to improve the photocatalytic performance of pure CdS, such as high recombination rate of photoinduced electron-hole pairs and photocorrosion. To solve these problems, a great many strategies have been therefore developed to enhance the photocatalytic activity of CdS, including synthesis of CdS quantum dots,[31, 32] deposition of noble metallic

nanoparticles[33, 34] formation of heterogeneous semiconductors,[35, 36] and modification with carbon nanomaterials.[37-39]

Among various carbon materials, graphene (GR), as a single layer of carbon atoms densely packed in a honeycomb two-dimensional (2D) lattice, has recently emerged as nanobuilding block for fabrication of various nanomaterials due to its unique sheet morphology, ultrahigh electron conductivity and mobility.[40,41] More recently, GR-semiconductor nanocomposites have been evidenced to be efficient photocatalysts on account of the imperative role of GR as electron acceptor/transportor which remarkably reduces the recombination rate of photoexcited electron-hole pairs.[42-48] Among which, intriguingly, GR-CdS nanocomposites have gained increasing attention for a wide range of photocatalytic applications.[42, 43, 47 46, 48] Although there have been some reports on the preparation of GR-CdS nanocomposites, it should be noted that most of the synthetic protocols developed by previous works are primarily confined to single hydrothermal method using toxic organic system. Moreover, previous investigations on GR-CdS nanocomposite mainly focus on liquid-phase degradation of pollutants or hydrogen production,[30, 37, 48] and the utilization of GR-CdS nanocomposite for photocatalytic selective organic transformation is relatively seldom reported. Furthermore, noteworthily, there is still a paucity of reports on the synthesis of GR-CdS nanocomposite *via* different strategies accompanied by their systematic comparison regarding the photocatalytic performances toward selective organic transformation under ambient conditions.

Herein, we have developed different methods to fabricate GR-CdS nanocomposites in which varied interfacial contact between GR and CdS components was tuned, and photocatalytic performances of these GR-CdS nanocomposites were simultaneously probed. It was found that the GR-CdS nanocomposites can be utilized as efficient visible-light-driven photocatalysts for

photocatalytic selective oxidation of benzyl alcohol to benzaldehyde under ambient conditions, as a result of synergistic interaction between GR and CdS ingredients. The influences of loading amount of GR and synthetic methods on the photocatalytic performances of GR-CdS nanocomposite were specifically explored, and photocatalytic mechanism was presented accordingly. It was found that introduction of GR is beneficial for the separation of photogenerated electron-hole charge carriers over GR-CdS nanocomposite and improving photostability of CdS. It is anticipated that our current work could provide new insights for the fabrication of GR-based semiconductor nanocomposites for a wide range of selective oxidation reactions.

2. Experimental Section

2.1 Materials

Cadmium chloride ($CdCl_2 \cdot 2.5H_2O$), thiourea (N_2H_4CS), ethylene glycol ($C_2H_6O_2$), graphite powder, sulfuric acid (H_2SO_4), nitric acid (HNO_3), hydrochloric acid (HCl), potassium persulfate ($K_2S_2O_8$), phosphorus pentoxide (P_2O_5), deionized water (DI H_2O, Milipore, 18.2 MΩ·cm resistivity), hydrogen peroxide (30 %, H_2O_2), N. N-Dimethylformamide (DMF), 3-aminopropyl-trimethoxysilane (ATPES), potassium permanganate ($KMnO_4$), and ethanol (C_2H_6O) were obtained from Sinopharm Chemical Reagent *Co.*, Ltd. (Shanghai, China). All reagents were analytical grade and used without further purification.

2.2 Preparation

The GR-CdS nanocomposites were fabricated by a facile hydrothermal method, the detailed synthetic route was vividly illustrated in **Scheme 1**. *(a) Fabrication of CdS and Graphene Oxide*

(GO) building blocks. CdS microspheres were prepared *via* a facile hydrothermal method, and GO was synthesized from natural graphite powder by a modified Hummers method. The synthetic details of CdS microspheres and GO are provided in the *Supporting information*. *(b) Synthesis of GR-CdS nanocomposites.* CdS microspheres were added into GO aqueous solution (5 mg/mL, pH = 6) with weight addition ratio of GO to CdS at 1 : 0.05 under vigorous stirring. After stirring for 30 min, the mixture was centrifuged and washed for several times with DI H_2O. Afterwards, GO-CdS (0.2 g) mixture dispersed in 80 mL of DI H_2O was transferred to Teflon-lined stainless steel vessel (100 mL) and autoclaved at 120 °C for 12 h. The obtained dark green precipitates were collected, washed thoroughly with DI H_2O, and dried in oven at 60°C. GR-CdS nanocomposite with 5 % (weight percentage) of GR by above hydrothermal approach was designated as 5GC-H. For comparison, 5 % GR-CdS nanocomposites synthesized by other methods, *i.e.* electrostatic self-assembly, refluxing at low temperature, and *in-situ* synthesis approach, were also fabricated and labeled as 5GC-E, 5GC-R, and 5GC-I, respectively. The details of the typical process for preparation of 5GC-E, 5GC-R and 5GC-I were elucidated and depicted in the *Supporting information (**Scheme S1**)*.

2.3 Characterization

The crystal phases of the samples were analyzed with a Bruker D8 Advance X-ray diffractometer (XRD) using Ni-filtered Cu Kα radiation at 40 kV and 40 mA. The optical properties of the samples were measured by a Cary 500 UV-visible diffuse reflectance spectrophotometer (DRS), in which $BaSO_4$ was employed as the internal reflectance standard. Field-emission scanning electron microscopy (FESEM, FEI Nova NANOSEM 230) was used to determine the morphologies of samples. Transmission electron microscopy (TEM) and high-resolution TEM (HRTEM) images were obtained using a JEOL model JEM 2010 EX instrument at an

accelerating voltage of 200 kV. Raman spectroscopic measurements were performed on a Renishaw inVia Raman System 1000 with a 532 nm Nd: YAG excitation source at room temperature. The Brunauer-Emmett-Teller (BET) specific surface area (S_{BET}) was analyzed by nitrogen adsorption in a Micromeritics ASAP 2020 apparatus. The photoluminescence (PL) spectra for solid samples were investigated on an Edinburgh FL/FS900 spectrophotometer. The electrochemical analysis was carried out in a conventional three-electrode cell using Pt plate and Ag/AgCl electrode as the counter electrode and reference electrode, respectively. The electrolyte was consisted of 0.2 M Na_2SO_4 aqueous solution (pH = 6.8). The working electrode was fabricated by a doctor-blade method and its exposed area was 0.25 cm^2. The photocurrent measurements were performed in a homemade three-electrode quartz cell with a PAR VMP3 Multi Potentiotat apparatus. The electrochemical impedance spectroscopy (EIS) experiments were conducted on a Precision PARC workstation.

2.4 Photocatalytic activity

Photocatalytic selective oxidation of benzyl alcohol to benzaldehyde was used as probing reaction. Firstly, mixture of benzyl alcohol (0.1 mmol) and catalyst (8 mg) was dissolved in 1.5 mL of benzotrifluoride (BTF), which was saturated with pure molecular oxygen.[49] The choice of solvent BTF is owing to its inertness to oxidation and high solubility for molecular oxygen.[49] Afterwards, the above mixture was transferred into a Pyrex glass bottle (10 mL) filled with molecular oxygen at a pressure of 0.1 MPa and stirred for 1.5 h to make the catalyst blend evenly in the solution. The samples were subsequently irradiated by a 300W Xe arc lamp (PLS-SXE 300, Beijing Trusttech Co. Ltd.) with a UV-CUT filter to cut off light of $\lambda < 420$ nm. After the reaction, the mixture was centrifuged at 12000 rmp for 20 min to completely remove the catalyst, and the remaining solution was analyzed with an Aglient Gas Chromatograph (GC-7820). The

assignment of products was confirmed by a Hewlett-Packard Gas Chromatograph/Mass Spectrometer (HP-5973GC/MS). Conversion of benzyl alcohol, yield of benzaldehyde, and selectivity for benzaldehyde were defined in the following:

$$Conversion\ (\%) = [(C_0 - C_{benzyl\ alcohol})/C_0] \times 100$$

$$Yield\ (\%) = C_{benzaldehyde}/C_0 \times 100$$

$$Selectivity\ (\%) = [C_{benzaldehyde}/(C_0 - C_{benzyl\ alcohols})] \times 100$$

where C_0 is the initial concentration of benzyl alcohol, $C_{benzyl\ alcohol}$ and $C_{benzaldehyde}$ are the concentration of the substrate benzyl alcohol and the corresponding benzaldehyde, respectively, at a certain time interval after photocatalytic reaction.

3. Results and discussion

The crystal phase properties of samples are probed by X-ray diffractometer (XRD). It can be seen from **Figure 1a** that GR-CdS nanocomposites with different weight addition ratios of GR display good crystallinity and the distinct diffraction peaks at 2θ values of 24.8°, 26.5°, 28.2°, 36.6°, 43.7°, 47.8° and 51.8° can be attributed to the (100), (002), (101), (102), (110), (103) and (112) crystal planes of stable hexagonal CdS phase (JCPDS No. 41-1049), respectively. However, there is no apparent peak for GR in the XRD patterns of GR-CdS nanocomposites which can be ascribed to two probable reasons. One is that the relatively low diffraction intensity of GR at 26.0° might be shielded by the predominant peak of hexagonal CdS phase at 26.5°.[48] The other is probably ascribed to the disappearance of the layer-stacking regularity after redox of graphite.[37] The XRD patterns of blank GO and GR are also shown in the inset of **Figure 1a**, from which it is clear to see that GO shows a sharp diffraction peak at 2θ of 10.1°. With regard to GR prepared by hydrothermal reduction, a very broad diffraction peak at 2θ value of 26.0° appears and the

diffraction peak at 2θ value of 10.1° for GO disappears completely, thus suggesting GO sheets have been wholly transformed to GR through facile hydrothermal reaction in our system. **Figure 1b** shows the Raman spectra of GO, graphite (GP) and 5 % GR-CdS nanocomposite, from which two distinct peaks located at *ca.* 1350 cm^{-1} and 1595 cm^{-1} were clearly observed for both GO and 5 % GR-CdS nanocomposite, which are attributed to D band and G band, respectively. Notably, I_D/I_G is normally utilized to measure the relative concentration of sp^3 hybridized defects relative to the sp^2 hybridized GR domains.[18, 50] As displayed in **Figure 1b**, I_D/I_G ratio for 5 % GR-CdS nanocomposite is determined to be 0.98 which is lower than that for GO (1.04), indicating lower defect density of GR-CdS nanocomposites as compared to GO.[51] Besides, according to the Raman spectrum of GP (**Figure 1b**), we can ascertain the formation of GR rather than GP in the GR-CdS nanocomposites.

The successful reduction of GO to GR can be further evidenced by the high-resolution C 1s XPS spectra of GO and 5% GR-CdS (5GC-H) nanocomposite, as demonstrated in **Figure 2**. High-resolution spectrum of C 1s for GO (**Figure 2a**) indicates the existence of various oxygen–containing functional groups on the GO surface. However, as displayed in **Figure 2b**, substantial loss of oxygen–containing functional groups was apparently observed in the high-resolution spectrum of C1s for 5% GR-CdS (5GC-H) nanocomposite, which strongly implies reduction of GO to GR after hydrothermal treatment.[18, 50-52]

UV-vis diffuse reflectance spectra (DRS) are used to determine the optical properties of the samples. It can be seen from **Figure 3a** that introduction of different weight addition ratio of GR exerts profound effect on the light absorption of the GR-CdS nanocomposites. With the GR content increasing, remarkably enhanced absorbance in the visible region ranging from 500 to 800 nm was apparently observed, which is in faithful agreement with the color change of the

samples. A plot obtained *via* the transformation based on the Kubelka-Munk function *versus* the energy of light is displayed in **Figure 3b**. The estimated band gap values of the samples are *ca.* 2.4, 2.36, 2.30, and 2.33 eV approximately, corresponding to blank-CdS, 1% GR-CdS, 5% GR-CdS, and 10% GR-CdS nanocomposite, respectively. These results indicate a band gap narrowing of CdS and enhanced visible light absorption due to the integration of 2D GR sheets in GR-CdS nanocomposites, which provides more intimate contact between light and the samples, and therefore facilitates the transfer of photogenerated charge carriers transfer across the interface.[18]

Field-emission scanning electron microscopy (FESEM) images are harnessed to directly analyze the microscopic structure of the samples, as displayed in **Figure 4**. It can be seen from **Figure 4a-d** that blank CdS with spherical plum-like and petalous morphology demonstrates average diameter of 1μm approximately (**Figure S1**). When CdS was integrated with GO, morphology of CdS was retained (**Figure 4a**), indicating hydrothermal treatment did not alter the original morphology of CdS. Alternately, FESEM results reveal intimate interfacial contact between CdS microspheres and GR sheets in which CdS nanospheres were closely enwrapped by GR scaffold.

The microscopic morphology of the samples was further analyzed by transmission electron microscopy (TEM), as shown in **Figure 5**. **Figure 5a** shows that blank CdS exhibit characteristic microsphere morphology and flower-like buildup with average diameter of *ca.* 1μm (**Figure 5b**) which is in accordance with FESEM result (**Figure 4a** & **Figure S1**). The morphologies of 5 % GR-CdS nanocomposite are shown in **Figure 5c-e**. It can be seen from **Figure 5d-e** that CdS was indeed closely enwrapped by GR sheets giving rise to intimate interfacial contact between them. In addition, the lattice spacing of 5 nm revealed in high-resolution TEM (HRTEM) image

(**Figure 5f)** is identified to be around 0.316 nm corresponding to the (101) crystallographic facet of CdS. The selected area electron diffraction (SAED) patterns, as displayed in the insets of **Figure 5f**, indicate that CdS possesses a single-crystalline wurtzite structure which is consistent with XRD result (**Figure 1**).[53]

The photocatalytic performance of the samples was evaluated by selective oxidation of benzyl alcohols to benzaldehyde under visible light irradiation. Blank experiments (without light or irradiation, **Figure S2**) disclose that no distinct photoactivity was observed over 5 % GR-CdS nanocomposite, thereby suggesting the reaction was truly driven by a photocatalytic process. As shown in **Figure 6a**, when 1 % GR was integrated with CdS, the conversion of benzyl alcohol, selectivity and yield of benzaldehyde over GR-CdS nanocomposite significantly increase than those over blank CdS. When the weight addition ratio of GR was increased to 5 %, optimal photocatalytic performance was achieved, for which conversion, selectivity, and yield over GR-CdS nanocomposite reach the highest values among all the samples. Specifically, 65 % conversion of benzyl alcohol and 52 % yield of benzaldehyde were attained over the 5 % GR-CdS nanocomposite, but only 7.7 % conversion and 4.7 % yield were reached over blank CdS. Obviously, 5 % GR-CdS nanocomposite is about 7 times higher than blank CdS for the enhanced photoactivity. Additional increase of GR percentage in GR-CdS nanocomposite leads to a deterioration of the photocatalytic performance. In this case, over deep oxidation of aldehyde may occur, thus leading to the decrease in selectivity, as reflected by the case of 10 % GR-CdS nanocomposite. Moreover, it should be particularly pointed out that more adding amount of GR (> 5 %) may also block the light absorption of CdS and weaken interfacial integration between them, therefore further resulting in the undesirable photoactivity.

Apart from photocatalytic activity, stability of photocatalyst is also of paramount importance

for its sustainable reuse.[54] **Figure 6b** displays the recycling measurements of selective oxidation of benzyl alcohol over 5 % GR-CdS nanocomposite under visible light irradiation (λ > 420 nm), which reveals that no noticeable loss in photoactivity was observed after four successive recyclings, hence suggesting the 5 % GR-CdS nanocomposite can serve as stable photocatalyst.

In order to determine the role of specific active species in the photocatalytic process, a series of control experiments using different radical scavengers for selective oxidation of alcohols over blank CdS and 5 % GR-CdS nanocomposite under visible light irradiation were performed, as clearly displayed in **Figure 7**. Various radical scavengers, such as *tert*-butyl alcohol (TBA) for hydroxyl radicals (·OH),[52, 55] ammonium oxalate (AO) for holes (h^+),[52, 55, 56] $AgNO_3$ for electrons (e^-) [54] and benzoquinone (BQ) for superoxide radicals ($O_2^{\cdot-}$)[57, 58] was added separately into the reaction system. As shown in **Figure 7a**, when ammonium oxalate (AO) scavenger for holes was added, the conversion of benzyl alcohol and yield of benzaldehyde over 5 % GR-CdS nanocomposite decrease under visible light irradiation. When benzoquinone (BQ) scavenger for superoxide radicals was added into the reaction system, the conversion and yield were significantly inhibited. Such a remarkable inhibition on conversion and yield was also observed when $AgNO_3$ was added into the reaction system. The result suggests that $O_2^{\cdot-}$, electrons (e^-), and holes (h^+) play the dominant role for the enhanced photocatalytic performance of 5 % GR-CdS nanocomposite. However, notably, negligible inhibition of conversion and yield over 5 % GR-CdS nanocomposite was observed when *tert*-butyl alcohol (TBA) scavenger for hydroxyl radicals (·OH) was added, indicating hydroxyl radicals (·OH) does not play predominant role in the photocatalytic proce. In addition, similar result was also observed over blank CdS (**Figure 7b**).

To disclose the origin accounting for the significantly enhanced photocatalytic performance

of hybrid nanocomposite toward selective oxidation reactions, adsorption property, specific surface area and photoelectronchemical properties of 5 % GR-CdS nanocomposite have therefore been explored. As demonstrated in **Figure S3**, 5 % GR-CdS nanocomposite exhibits only a little larger adsorbability for benzyl alcohol in the dark, which may be attributed to its higher specific surface area as compared with blank CdS (**Table S1**). Therefore, it can be speculated that the superior photocatalytic performance of 5 % GR-CdS nanocomposite to CdS does not arise mainly from their differences in adsorption and specific surface area.

Figure 8a shows transient photocurrent responses of the samples over several on–off cycles under visible light irradiation ($\lambda > 420$ nm). It is clear to see that addition of GR remarkably enhance the photocurrent of GR-CdS nanocomposites, for which 5 % GR-CdS nanocomposite exhibits the most enhancement, thereby suggesting more efficient separation and longer lifetime of photoexcited electron-hole pairs over 5 % GR-CdS nanocomposite under visible light irradiation.

To further determine the advantage of 5 % GR-CdS nanocomposite over CdS in improving the transfer of photogenerated electron-hole charge carriers, electrochemical impedance spectra (EIS) of the electrodes under visible light irradiation were also measured. It can be seen from **Figure 8b** that 5 % GR-CdS nanocomposite shows shorter semi-circle as compared with blank CdS, which reveals a decrease in the solid state interface layer resistance and the charge transfer resistance on the surface.[71] Thus, it can be speculated that charge carriers transfer over 5 % GR-CdS nanocomposite is more efficient than that over blank CdS which remarkably boosts the photocatalytic efficiency. This can be further evidenced by PL analysis. It is known that PL spectra are often used to study the surface process involving the separation of electron-hole carriers on the semiconductor upon irradiation.[52, 55, 59]. **Figure 9a** shows the PL spectra of 5 %

GR-CdS nanocomposite at room temperature with an excitation wavelength of 460 nm. The origin of the characteristic wide PL band in the visible region is attributed to irradiative recombination of self-trapped excitons in CdS.[55] As displayed in **Figure 9a**, PL intensity of 5 % GR-CdS nanocomposite is much weaker than that of blank CdS, this might be resulted from the suppressed recombination of photoexcited electrons and holes *via* band-to-band emission transition, which is in favor of the photocatalytic reaction.[60] PL result manifests that the significantly enhanced photocatalytic performance of 5 % GR-CdS nanocomposite toward selective oxidation of benzyl alcohol to benzaldehyde can be attributed to the efficient separation of electron-hole pairs under visible light irradiation.[60-62] **Figure S4** exhibits the Mott-Schottky plots for the 5 % GR-CdS nanocomposite, in which positive slope of the C^{-2}-E plots reveals the expected n-type semiconductor of CdS in the composite.[62] The flatband potential of 5 % GR-CdS nanocomposite obtained by extrapolation of the Mott-Schottky plots is approximately equal to -0.60V,[63] which are more negative than the standard reduction potential of $O_2/O_2^{\cdot-}$ (-0.15 V *vs* NHE).[14] Thus it is thermodynamically permissible for the photogenerated electrons to transfer to the absorbed O_2 producing the superoxide radicals ($O_2^{\cdot-}$). Therefore, it can be concluded that integration of CdS with GR improve the transfer of photogenerated charge carriers, thus hampering the recombination rate of electron-hole pairs.

In order to evaluate the influence of interfacial contact between CdS and GR on the photocatalytic performance of the GR-CdS nanocomposite, GR-CdS binary nanocomposites with the same percentage of GR (5 %) were synthesized by different methods for systematic comparison (**Scheme S1**). The crystal phases of the samples (*i.e.* 5GC-E, 5GC-I and 5GC-R) were probed by XRD, as shown in **Figure S5**. It shows that the 5 % GR-CdS nanocomposite prepared by different methods demonstrate similar XRD patterns which can be concurrently

indexed to standard card (JCPDS card no. 41-1409). Selective oxidation of benzyl alcohol to benzaldehyde under visible light irradiation was utilized as probing reaction to evaluate the photocatalytic performances of 5GC-H, 5GC-E, 5GC-I and 5GC-R. Consistently, **Figure 9b** shows that 5GC-H exhibits the optimal photocatalytic activity among all the counterparts under otherwise the same experimental conditions and photocatalytic activity of the samples follows the order of: 5GC-H > 5GC-R > 5GC-E > 5GC-I. Thus, it can be concluded that 5GC-H obtained *via* hydrothermal reduction yields the most enhanced photoactivity toward selective oxidation reactions resulting from the most intimate contact between CdS and GR, which can be verified by the SEM result, as displayed in **Figure 4c** and **Figure S6e-g**. This can be further confirmed by the photoluminescence (PL) and EIS results. As displayed in **Figure 9c**, the obviously lower emission intensity of 5GC-H than those of 5GC-R, 5GC-I and 5GC-E demonstrates an effective interfacial charge-transfer process over 5GC-H. Consistently, EIS result (**Figure 9d**) shows that 5GC-H demonstrates the shortest semi-circle as compared with other counterparts, which once again evidences the most efficient charge transfer over 5GC-H.[64] Notably, the PL and EIS results are in faithful agreement with the photocatalytic performances of the samples (**Figure 9b**).

On the basis of the above analysis, a probable photocatalytic mechanism for GR-CdS nanocomposite was proposed and vividly illustrated in **Figure 10**. Under visible-light irradiation, electrons (e^-) are excited from the valence band (VB) of CdS to the its conduction band (CB), leaving the holes in the VB, thereby forming the electron–hole pairs. Meanwhile, the photogenerated electrons can rapidly transfer to the GR framework due to the intimate interfacial contact between CdS and GR and excellent electron conductivity of GR, thus resulting in significantly enhanced lifetime of photogenerated electron-hole charge carriers. Concurrently, with regard to the oxidation reaction, molecular oxygen in the reaction system can be activated by

reacting with the photogenerated electrons to form large amount of superoxide radicals ($O_2^{\cdot-}$), as evidenced by the control experiments in **Figure 6**. The benzyl alcohol adsorbed on the surface of GR-CdS nanocomposite can be subsequently oxidized by these active species (*e.g.* $O_2^{\cdot-}$) giving rise to the product of benzaldehyde. On the other hand, it should be emphasized that benzyl alcohols may also be oxided directly by the holes photogenerated from CdS to give the target product of benzaldehyde. Consequently, higher photocatalytic activity of GR-CdS nanocomposite can be ascribed to the synergistic effects of improved visible light absorption and prolonged lifetime of photogenerated electron-hole pairs, as a result of adding appropriate amount of GR in the nanocomposite which acts as efficient electron transporter and collector.

4. Conclusions

In summary, we have fabricated the well-defined GR-CdS nanocomposites by a facile and template-free hydrothermal approach, by which intimate interfacial contact between CdS and GR sheets are achieved. Compared to blank CdS, this large 2-D flat structure of GR-CdS nanocomposite provides remarkably enhanced separation photogenerated electron-hole pairs in which GR serve as efficient electron transporter and collector. Moreover, it was found that the as-prepared GR-CdS nanocomposite demonstrates excellent photocatalytic performance toward selective oxidation of benzyl alcohol to benzaldehyde and desirable photostability under visible light irradiation. Furthermore, photocatalytic performances of the GR-CdS nanocomposite prepared by different strategies were systematically compared which highlights the importance of interfacial contact between CdS and GR. It is anticipated that our current work could provide new insights to the synthesis of GR-based semiconductor nanocomposites in aqueous phase and offer new approach for exploration of the GR-based semiconductor nanocomposites for photocatalytic

selective organic transformation.

Acknowledgements

This work is financially supported by the Natural Science Foundation of Fujian, China 2011J05024)

References

1. D. Šojić, V. Despotović, B. Abramović, N. Todorova, T. Giannakopoulou and C. Trapalis, *Molecules*, 2010, **15**, 2994-3009.
2. S. Liu, J. Yu and M. Jaroniec, *J. Am .Chem. Soc.*, 2010, **132**, 11914-11916.
3. H. G. Yang, G. Liu, S. Z. Qiao, C. H. Sun, Y. G. Jin, S. C. Smith, J. Zou, H. M. Cheng and G. Q. Lu, *J. Am. Chem. Soc.*, 2009, **131**, 4078-4083.
4. M. Ni, M. K. H. Leung, D. Y. C. Leung and K. Sumathy, *Renewable and Sustainable Energy Reviews*, 2007, **11**, 401-425.
5. F. Iskandar, A. B. D. Nandiyanto, K. M. Yun, C. J. Hogan, K. Okuyama and P. Biswas, *Adv. Mater.*, 2007, **19**, 1408-1412.
6. J. H. Park, S. Kim and A. J. Bard, *Nano Lett.*, 2005, **6**, 24-28.
7. G. H. Liu, Y. F. Zhu, X. R. Zhang and B. Q. Xu, *Anal. Chem.*, 2002, **74**, 6279-6284.
8. R. D. Cortright, R. R. Davda and J. A. Dumesic, *Nature*, 2002, **418**, 964-967.
9. M. R. Hoffmann, S. T. Martin, W. Choi and D. W. Bahnemann, *Chem. Rev.*, 1995, **95**, 69-96.
10. A. J. Bard and M. A. Fox, *Acc. Chem. Res.*, 1995, **28**, 141-145.
11. B. O'Regan and M. Gratzel, *Nature*, 1991, **353**, 737-740.
12. A. Fujishima and K. Honda, *Nature*, 1972, **238**, 37-38.
13. M. Zhang, Q. Wang, C. Chen, L. Zang, W. Ma and J. Zhao, *Angew. Chem., Int. Ed.*, 2009, **48**, 6081-6084.
14. M. Zhang, C. Chen, W. Ma and J. Zhao, *Angew. Chem., Int. Ed.*, 2008, **47**, 9730-9733.
15. Y. Shiraishi and T. Hirai, *J. Photochem. Photobiol C： Photochem. Rev.*, 2008, **9**, 157-170.
16. Q. Wang, M. Zhang, C. Chen, W. Ma and J. Zhao, *Angew. Chem., Int. Ed.*, 2010, **49**, 7976-7979.

17. S. Higashimoto, N. Kitao, N. Yoshida, T. Sakura, M. Azuma, H. Ohue and Y. Sakata, *J. Catal.*, 2009, **266**, 279-285.

18. Y. Zhang, Z.-R. Tang, X. Fu and Y.-J. Xu, *ACS Nano*, 2011, **5**, 7426-7435.

19. J. M. Herrmann, J. Disdier and P. Pichat, *J. Phys. Chem.*, 1986, **90**, 6028-6034.

20. M. Matsumura, S. Furukawa, Y. Saho and H. Tsubomura, *J. Phys. Chem.*, 1985, **89**, 1327-1329.

21. P. Kumar, P. Singh and B. Bhattacharya, *Ionics*, 2011, **17**, 721-725.

22. J. Britt and C. Ferekides, *Appl. Phys. Lett.*, 1993, **62**, 2851-2852.

23. M. Tsuji, T. Aramoto, H. Ohyama, T. Hibino and K. Omura, *J. Cryst. Growth*, 2000, **214–215**, 1142-1147.

24. R.-M. Ma, L. Dai, H.-B. Huo, W.-J. Xu and G. G. Qin, *Nano Lett.*, 2007, **7**, 3300-3304.

25. Y. Lai, Y. Yu, P. Zhong, J. Wu, Z. Long and C. Liang, *Anal. Lett.*, 2006, **39**, 1201-1209.

26. J. Wang, G. Liu and A. Merkoçi, *J.Am.chem.soc.*, 2003, **125**, 3214-3215.

27. W. Zhao, Z. Bai, A. Ren, B. Guo and C. Wu, *Appl. Surf. Sci.*, 2010, **256**, 3493-3498.

28. J. Nayak, S. N. Sahu, J. Kasuya and S. Nozaki, *Appl. Surf. Sci.*, 2008, **254**, 7215-7218.

29. X. Zong, J. Han, G. Ma, H. Yan, G. Wu and C. Li, *J. Phys. Chem. C*, 2011, **115**, 12202-12208.

30. X. Zong, H. Yan, G. Wu, G. Ma, F. Wen, L. Wang and C. Li, *J. Am. Chem. Soc.*, 2008, **130**, 7176-7177.

31. M. H. Entezari and N. Ghows, *Ultrason. Sonochem.*, 2011, **18**, 127-134.

32.A. J. Hoffman, G. Mills, H. Yee and M. R. Hoffmann, *J. Phys. Chem.*, 1992, **96**, 5546-5552.

33. W.-T. Chen, T.-T. Yang and Y.-J. Hsu, *Chem. Mater.*, 2008, **20**, 7204-7206.

34. Y. Li, Y. Xie, S. Peng, G. Lu and S. Li, *Chemosphere*, 2006, **63**, 1312-1318.

35. H. Yan, J. Yang, G. Ma, G. Wu, X. Zong, Z. Lei, J. Shi and C. Li, *J. Catal.*, 2009, **266**, 165-168.

36. D. R. Baker and P. V. Kamat, *Adv. Funct. Mater.*, 2009, **19**, 805-811.

37. L. Jia, D.-H. Wang, Y.-X. Huang, A.-W. Xu and H.-Q. Yu, *J. Phys. Chem. C*, 2011, **115**, 11466-11473.

38. X. Li, Y. Jia and A. Cao, *ACS Nano*, 2009, **4**, 506-512.

39. L. Sheeney-Haj-Ichia, B. Basnar and I. Willner, *Angew. Chem., Int. Ed.*, 2005, **44**, 78-83.

40. A. K. Geim, *Science*, 2009, **324**, 1530-1534.

41. A. K. Geim and K. S. Novoselov, *Nat Mater*, 2007, **6**, 183-191.

42. F. Liu, X. Shao, J. Wang, S. Yang, H. Li, X. Meng, X. Liu and M. Wang, *J. Alloys Compd.*, 2013, **551**, 327-332.

43. S. Kaveri, L. Thirugnanam, M. Dutta, J. Ramasamy and N. Fukata, *Ceram. Int.*, 2013, **39**, 9207-9214.

44. Y. Zhang, J. Tian, H. Li, L. Wang, X. Qin, A. M. Asiri, A. O. Al-Youbi and X. Sun, *Langmuir*, 2012, **28**, 12893-12900.

45. J. Zhang, J. Yu, M. Jaroniec and J. R. Gong, *Nano Lett.*, 2012, **12**, 4584-4589.

46. A. Ye, W. Fan, Q. Zhang, W. Deng and Y. Wang, *Catal. Sci. Technol.*, 2012, **2**, 969-978.

47. S. Pan and X. Liu, *New J. Chem.*, 2012, **36**, 1781–1787.

48. Q. Li, B. Guo, J. Yu, J. Ran, B. Zhang, H. Yan and J. R. Gong, *J. Am.Chem. Soc.*, 2011, **133**, 10878-10884.

49. Z.-R. Tang, Y. Zhang and Y.-J. Xu, *ACS Appl. Mater. Interfaces*, 2012, **4**, 1512-1520.

50. Y. T. Liang, B. K. Vijayan, K. A. Gray and M. C. Hersam, *Nano Lett.*, 2011, **11**, 2865-2870.

51. Q. Huang, S. Tian, D. Zeng, X. Wang, W. Song, Y. Li, W. Xiao and C. Xie, *ACS Catal.*, 2013, **3**, 1477-1485.

52. Y. Zhang, N. Zhang, Z.-R. Tang and Y.-J. Xu, *ACS Nano*, 2012, **6**, 9777-9789.

53. Y.-F. Lin, J. Song, Y. Ding, S.-Y. Lu and Z. L. Wang, *Adv. Mater.*, 2008, **20**, 3127-3130.

54. L. -L, Ma, H. -Z. Sun, Y. -G. Zhang, Y. -L. Lin, J. -L. Li, E. -K Wang, Y. Yu, M. Tan and J. -B. Wang, *Nanotechnology*, 2008, **19**, 115709.

55. N. Zhang, Y. Zhang, M.-Q. Yang, Z.-R. Tang and Y.-J. Xu, *J. Catal.*, 2013, **299**, 210-221.

56. O. Carp, C. L. Huisman and A. Reller, *Prog. Solid State Chem.*, 2004, **32**, 33-177.

57. P. Raja, A. Bozzi, H. Mansilla and J. Kiwi, *J. Photochem. Photobiol., A*, 2005, **169**, 271-278.

58. M. Stylidi, D. I. Kondarides and X. E. Verykios, *Appl. Catal., B: Environme*, 2004, **47**, 189-201.

59. F. Xiao, *J. Phys. Chem. C*, 2012, **116**, 16487-16498.

60. S. Shen, L. Zhao, X. Guan and L. Guo, *J. Phys. Chem. Solids*, 2012, **73**, 79-83.

61. L. L. Chng, N. Erathodiyil and J. Y. Ying, *Acc. Chem. Res.*, 2013, **46**, 1825-1837.

62. N. Zhang, Y. Zhang, X. Pan, X. Fu, S. Liu and Y.-J. Xu, *J. Phys. Chem. C*, 2011, **115**, 23501-23511.

63. D.-S. Kong, *Langmuir*, 2008, **24**, 5324-5331.

64. B.-L. He, B. Dong and H.-L. Li, *Electrochem. Commun.*, 2007, **9**, 425-430.

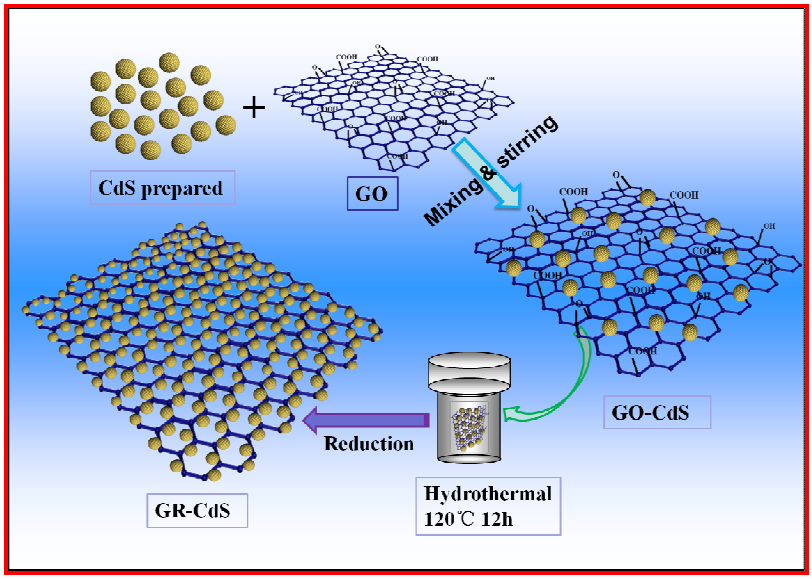

Scheme 1. Flowchart for preparation of GR-CdS nanocomposites.

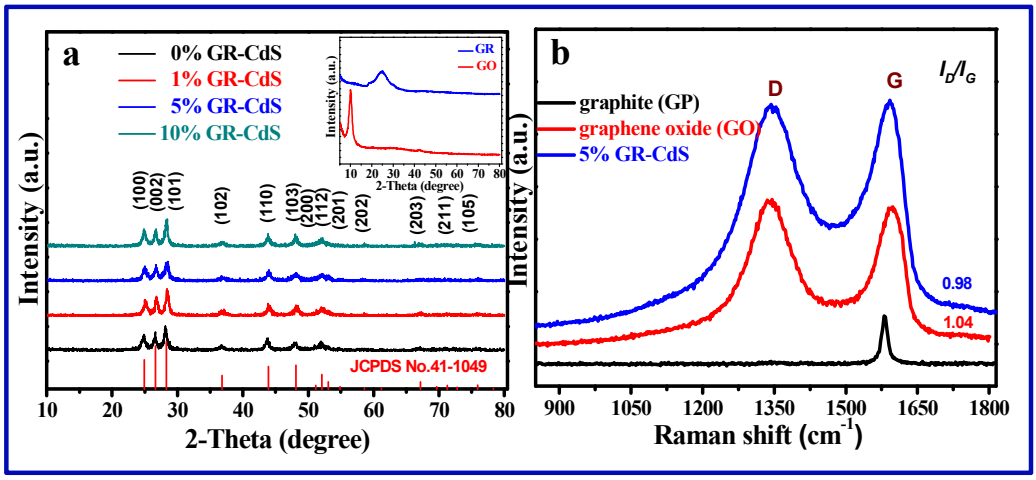

Figure 1. XRD patterns of (a) GR-CdS nanocomposites with different weight addition ratio of GR together with XRD patterns of GO and GR in the inset, and (b) Raman spectra of GP, GO and 5 % GR-CdS nanocomposite.

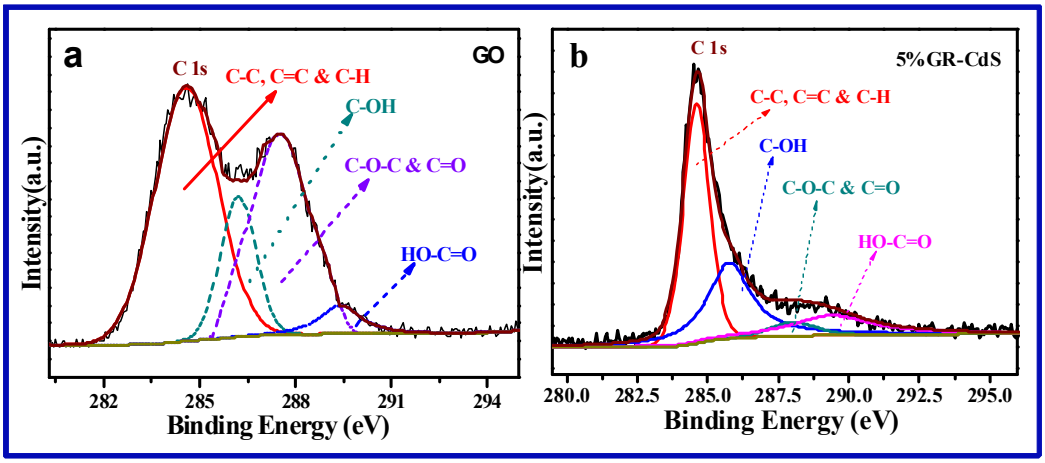

Figure 2. High-resolution XPS spectra of C 1s for (a) GO and (b) 5 % GR-CdS nanocomposite.

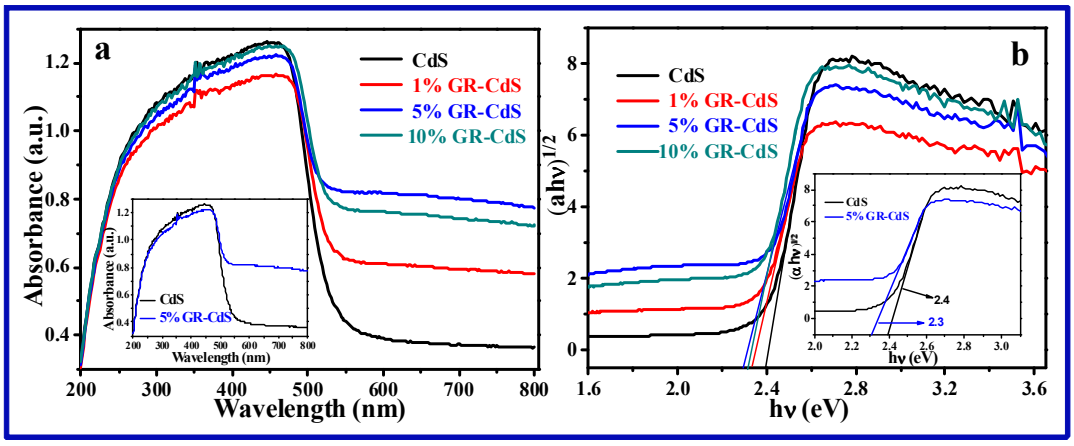

Figure 3. UV-vis diffuse reflectance spectra (DRS) of (a) GR-CdS nanocomposites with different weight addition ratio of GR to CdS, and (b) plot of transformed Kubelka-Munk function *versus* the energy of light.

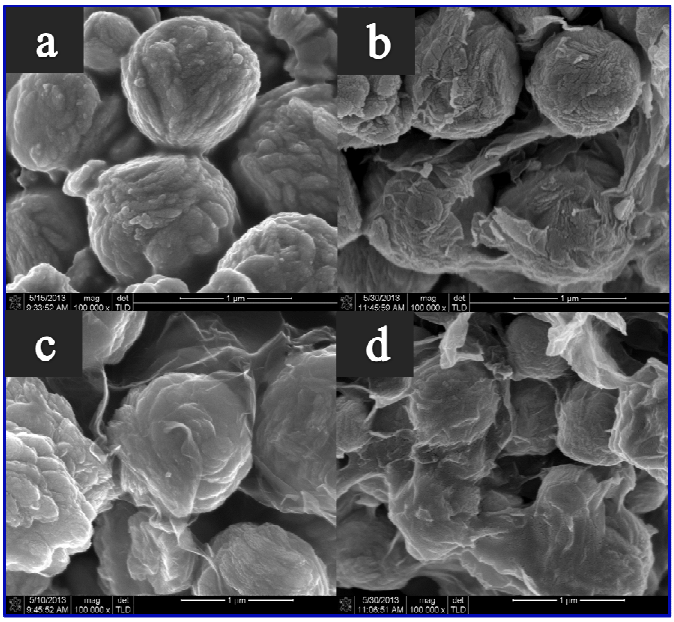

Figure 4. FESEM images of (a) CdS microsphere, (b) 1% GR-CdS, (c) 5 % GR-CdS, and (d) 10 % GR-CdS nanocomposites.

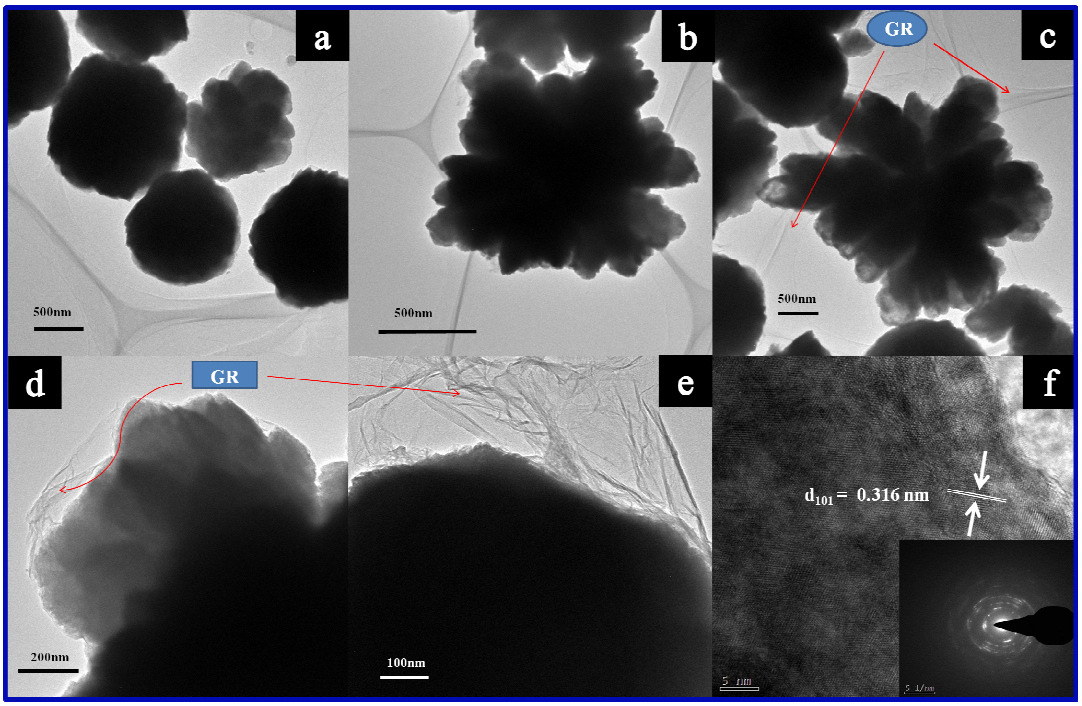

Figure 5. TEM images of blank CdS (a & b), (c-e) TEM images and (f) HRTEM images of 5 % GR-CdS nanocomposite with SAED pattern in the inset.

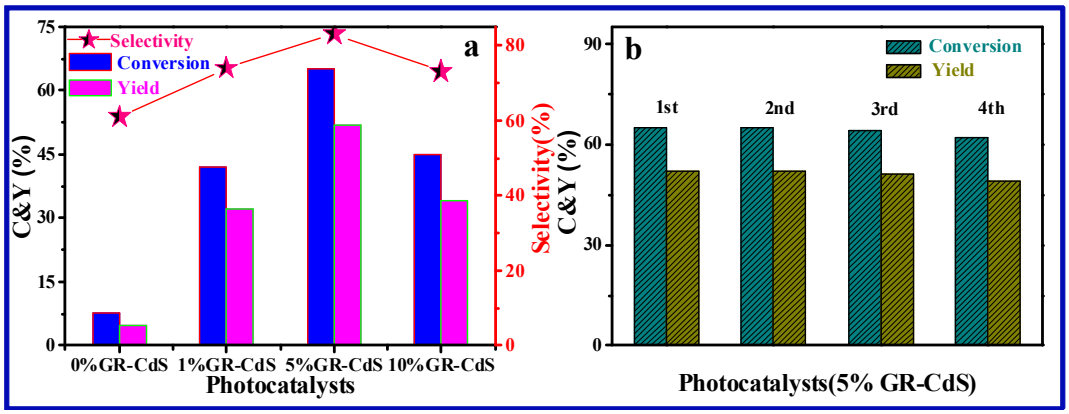

Figure 6. (a) Photocatalytic selective oxidation of benzyl alcohol to benzaldehyde under visible light irradiation (λ > 420 nm) for 2 h over GR-CdS nanocomposites with different weight addition ratio of GR. Note: C & Y are the abbreviation for conversion and yield, respectively. (b) Cycling photocatalytic selective oxidation of benzy lalcohol to benzaldehyde over 5 % GR-CdS nanocomposite under visible light irradiation (λ > 420 nm) for every 2 h.

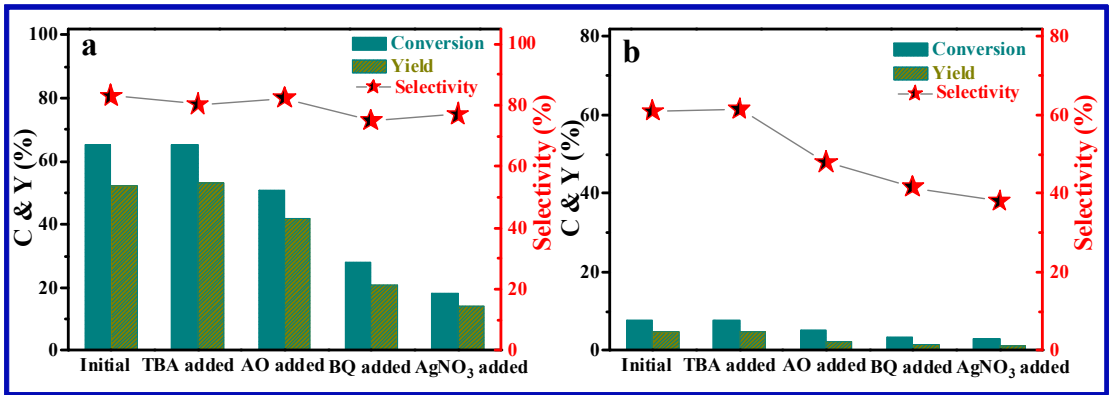

Figure 7. Control experiments using different radical scavengers in the photocatalytic selective oxidation of benzyl alcohol over (a) 5 % GR-CdS nanocomposite and (b) blank CdS in BTF solvent under visible light irradiation (λ > 420 nm) for 2 h. Note: C & Y are the abbreviation for conversion and yield, respectively.

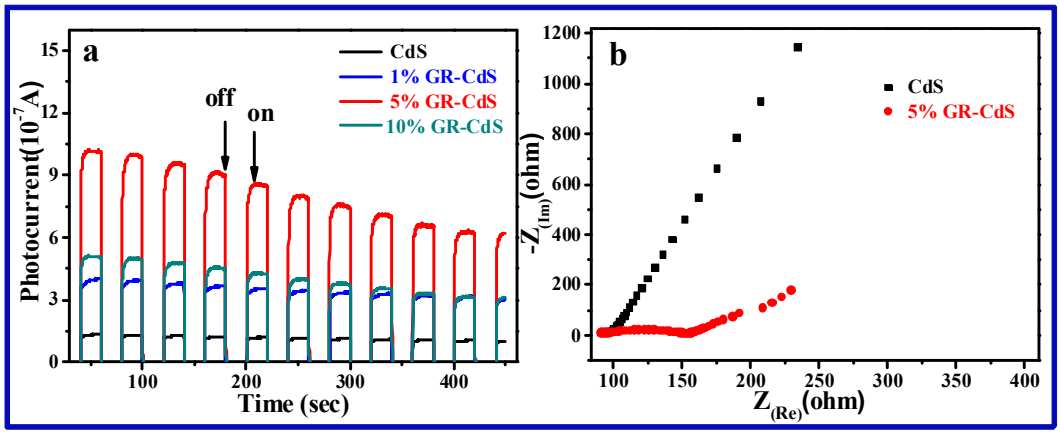

Figure 8. (a) Transient photocurrent responses of blank CdS and GR-CdS nanocomposites with different weight addition ratio of GR, and (b) Nyquist impedance plots of blank CdS and 5 % GR-CdS nanocomposite in 0.2 M Na_2SO_4 aqueous solution without bias *versus* Ag/AgCl (pH = 6.8) under visible light (λ > 420 nm) irradiation.

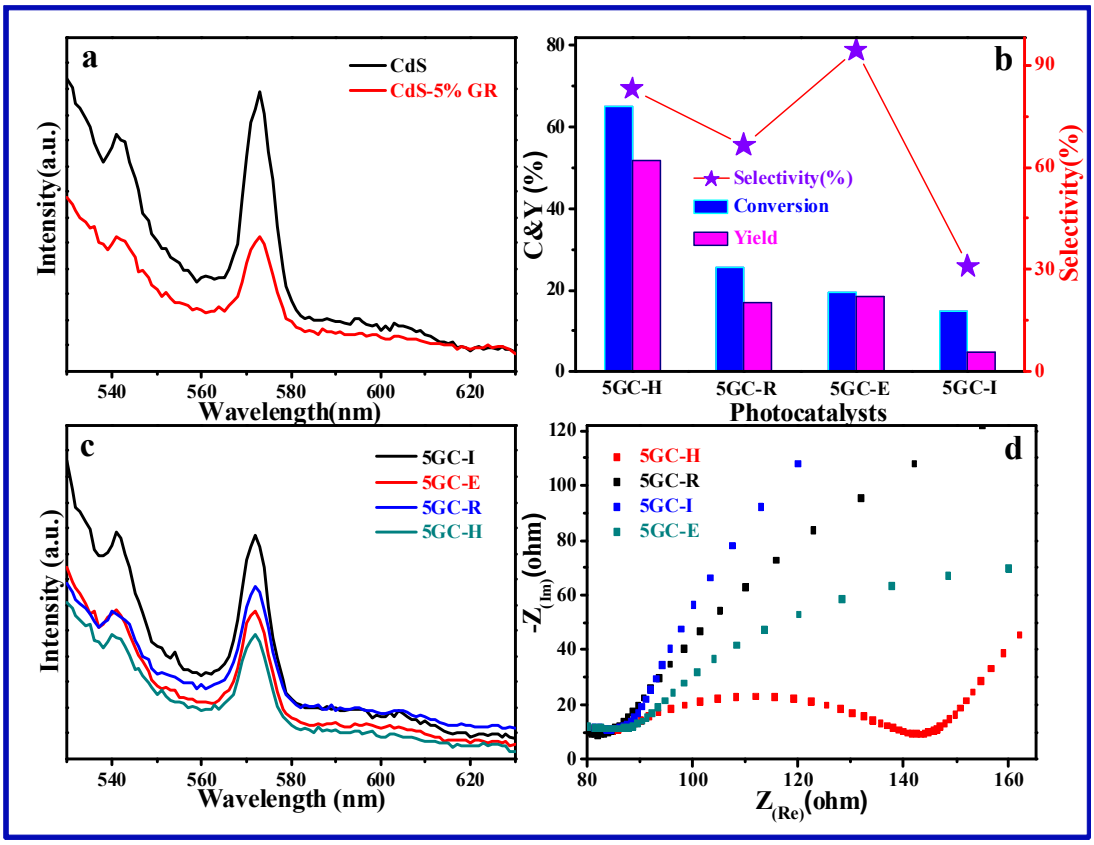

Figure 9. (a) Photoluminescence (PL) spectra of blank CdS and 5 % GR-CdS nanocomposite, and (b) photocatalytic selective oxidation of benzyl alcohol to benzaldehyde under visible light irradiation (λ > 420 nm) for 2 h over various 5 % GR-CdS nanocomposite prepared by different methods. Note: C & Y are the abbreviation for conversion and yield, respectively. (c) Photoluminescence (PL) specta and (d) Nyquist impedance plots of various 5 % GR-CdS nanocomposites prepared by different methods.

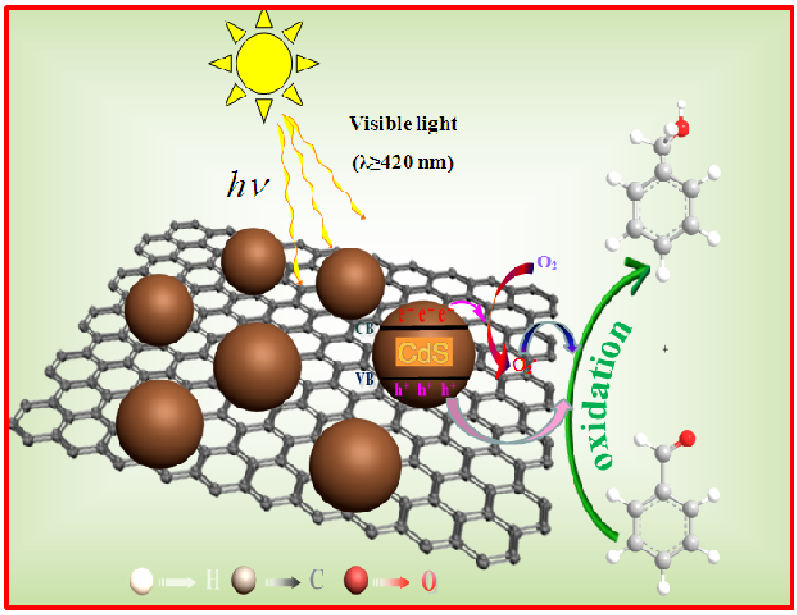

Figure 10. Schematic illustrating the photocatalytic mechanism for selective oxidation of benzyl alcohol to benzaldehyde over the GR-CdS nanocomposite.

Table of Contents Graphic